Available online at www.sciencedirect.com
SCIENCE DIRECT®
Journal of Contaminant Hydrology 70 (2004) 249–269
JOURNAL OF Contaminant Hydrology
www.elsevier.com/locate/jconhyd

Reactive transport modelling of biogeochemical processes and carbon isotope geochemistry inside a landfill leachate plume

Boris M. van Breukelen[a,*], Jasper Griffioen[b], Wilfred F.M. Röling[c], Henk W. van Verseveld[c,1]

[a] *Department of Hydrology and Geo-Environmental Sciences, Faculty of Earth and Life Sciences, Research School NSG, Vrije Universiteit, De Boelelaan 1085, NL-1081 HV Amsterdam, The Netherlands*
[b] *Netherlands Institute of Applied Geosciences TNO, Princetonlaan 6, NL-3508 TA Utrecht, The Netherlands*
[c] *Section Molecular Microbial Ecology, Department of Molecular Cell Physiology, Faculty of Earth and Life Sciences, Research School SENSE, Vrije Universiteit, De Boelelaan 1085, NL-1081 HV Amsterdam, The Netherlands*

Received 11 July 2002; received in revised form 3 September 2003; accepted 12 September 2003

Abstract

The biogeochemical processes governing leachate attenuation inside a landfill leachate plume (Banisveld, the Netherlands) were revealed and quantified using the 1D reactive transport model PHREEQC-2. Biodegradation of dissolved organic carbon (DOC) was simulated assuming first-order oxidation of two DOC fractions with different reactivity, and was coupled to reductive dissolution of iron oxide. The following secondary geochemical processes were required in the model to match observations: kinetic precipitation of calcite and siderite, cation exchange, proton buffering and degassing. Rate constants for DOC oxidation and carbonate mineral precipitation were determined, and other model parameters were optimized using the nonlinear optimization program PEST by means of matching hydrochemical observations closely (pH, DIC, DOC, Na, K, Ca, Mg, NH_4, Fe(II), SO_4, Cl, CH_4, saturation index of calcite and siderite). The modelling demonstrated the relevance and impact of various secondary geochemical processes on leachate plume evolution. Concomitant precipitation of siderite masked the act of iron reduction. Cation exchange resulted in release of Fe(II) from the pristine anaerobic aquifer to the leachate. Degassing, triggered by elevated CO_2 pressures caused by carbonate precipitation and proton buffering at the front of the plume, explained the observed downstream decrease in methane concentration.

* Corresponding author. Tel.: +31-20-444-7393; fax: +31-20-444-9940.
E-mail address: boris.van.breukelen@falw.vu.nl (B.M. van Breukelen).

[1] Unfortunately, Henk died on 11 July 2003. He was an associate professor of Molecular Microbial Ecology and Industrial Microbiology. In remembrance of a mentor, a fine colleague and friend.

doi:10.1016/j.jconhyd.2003.09.003

Simulation of the carbon isotope geochemistry independently supported the proposed reaction network.

Keywords: Reactive transport; Modelling; Natural attenuation; Biogeochemistry; Landfill, ^{13}C

1. Introduction

Natural attenuation (NA) processes are able to restrict the spreading of organic pollution in aquifers (e.g., Christensen et al., 2001). However, uncertainty about the continuation of NA necessitates a continuous monitoring. Monitored natural attenuation (MNA) is therefore an emerging remediation technique. Predictive models on plume evolution may reveal important processes and factors that control NA and can thereby guide and optimize the monitoring. Modelling and data gathering should therefore be considered as an iterative process. Besides the occurrence, also the type, the kinetics and sustainability of the governing degradation reactions should be determined. The type of degradation process (e.g., aerobic, nitrate reduction, iron reduction, etc.) changes in time and space as reflected by a sequence of redox zones observed from the source zone to the outskirts of an organic pollution plume (e.g., Christensen et al., 2000, 2001). Prediction of the redox chemistry is essential, since the extent of degradation of specific organic pollutants depends on the associated redox process (Krumholz et al., 1996; Christensen et al., 2000, 2001).

Constraining a reactive transport model to site-specific observations enables quantification of redox processes and prediction of plume evolution. Various reactive transport model codes have been developed in the last decade (Essaid et al., 1995; Clement et al., 1998; Abrams and Loague, 2000a; Murphy and Ginn, 2000; Islam et al., 2001; Van der Lee and de Windt, 2001; Brun and Engesgaard, 2002). A reactive transport model should include in addition to the primary degradation reactions (e.g., degradation of organic carbon coupled to iron reduction) also secondary redox (e.g., Fe(II) oxidation) and other geochemical reactions (e.g., cation exchange, siderite precipitation) in order to constrain the redox equations, since these reactions affect concentrations of redox species and pH as well (Hunter et al., 1998). This intrinsic capability makes multicomponent geochemical transport models superior to multiple solute transport models.

Several studies exist where reactive transport models were used to model field observations in aquifers contaminated by point sources of organic pollution (Essaid et al., 1995; Prommer et al., 1999; Abrams and Loague, 2000b; Mayer et al., 2001; Brun et al., 2002). Modelling the biogeochemical reactions in a landfill leachate plume seems especially complicated because of the diversity of solutes and processes involved, and has been performed only recently (Brun et al., 2002). Brun et al. (2002) incorporated Monod kinetics with biomass growth for five bacterial populations equal to the number of redox zones to simulate the degradation of dissolved organic carbon (DOC), but were less ambitious with respect to simulating the complexity of the geochemical system. The discrepancy between the model and observations (e.g., pH, bicarbonate, Fe(II)) was attributed to uncertainty on initial conditions (DOC concentration, iron oxide content), a high yield factor for microbial growth, and omission of siderite precipitation.

The present study illustrates that simulation of various secondary geochemical processes (cation exchange, proton buffering, kinetic precipitation of carbonate minerals, and degassing) is required to provide a possible explanation of the observed downstream improvement in leachate composition along a central flow path in an iron-reducing landfill leachate plume (Banisveld landfill, the Netherlands). The model includes simulation of the carbon-13 isotope geochemistry of the plume in order to verify model results. First-order DOC degradation was applied instead of Monod kinetics with biomass growth, in order to reduce the number of sensitive and unknown parameters (Essaid et al., 1995; Keating and Bahr, 1998). Rate constants for DOC oxidation, and calcite/siderite precipitation were calibrated, while other model parameters were optimized using the nonlinear optimization program PEST (Watermark Numerical Computing, http://www.sspa.com/pest).

2. Construction of the reactive transport model

2.1. Banisveld landfill research site

The Banisveld landfill (6 ha) is situated 5 km southwest of Boxtel, the Netherlands. Disposal of primarily household refuse occurred in a former 6-m-deep sandpit between 1965 and 1977. Artificial or natural liners are absent, while most of the waste is present below the groundwater table, which lies less than 2 m below surface. The hydrogeochemistry of the site is described in Van Breukelen et al. (2003). Here, only a brief summary will be given. A leachate plume was detected using cone penetration tests at a depth of about 4 to 9 m below surface to a distance of about 70 m from the landfill border (Fig. 1). The plume migrates through a heterogeneous phreatic aquifer, which consists of fine- to coarse-grained unconsolidated clayey sands. Groundwater observation wells

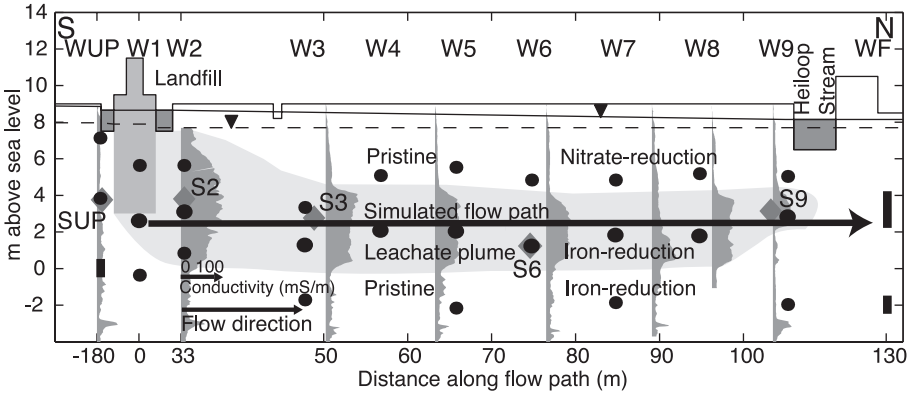

Fig. 1. Cross section of the research transect downstream of the landfill site. The leachate plume is depicted in light gray and delineated using the formation conductivity, which is plotted from left to right (dark gray). The position of the groundwater observation wells (WUP, W1–W9, WF: black dots or vertical lines), sediment samples (SUP, S2, S3, S6, S9: ♦), the minimum and maximum observed hydraulic head (▼), and the simulated flow path are shown.

(WUP, W1–W9, WF) were placed in the direction of groundwater flow within and around the plume (Fig. 1). At each well site two or three wells were placed with 20-cm length screens at different depths. Wells are indicated by the following notation: Wxy, where x is the code of the observation well site (UP, 1–9, F), and y refers to the screen depth of a well at well site x (a—upper screen (generally above plume); b—middle screen (inside plume); c—lower screen (below plume)). Sampling and analysis of groundwater were performed in June 1998, September 1998 and October 1999. Sediment samples were taken at five locations (SUP, S2, S3, S6, and S9; see Fig. 1) at plume depth for geochemical analysis in October 1998.

2.2. Model code

The 1D PHREEQC-2 model code (Parkhurst and Appelo, 1999) was used to simulate the evolution of groundwater quality along the central flow path in the leachate plume (Fig. 1). The PHREEQC database provided equilibrium constants for acid–base reactions, complexation of inorganic species, and the solubility of minerals and gases (CH_4, CO_2). Solubility of Ar and N_2 were taken from Andrews (1992). The possible contribution of dissolved organic carbon (DOC) to alkalinity was neglected (< 2%; Van Breukelen et al., 2003).

Simulation of 1D transport was appropriate, because no dilution of leachate occurred along the flow path (Van Breukelen et al., 2003): chloride concentrations in leachate were much higher than in pristine groundwater (Table 1) and remained constant in the flow direction (Fig. 5). The model assumes that the leachate composition in downstream wells W2 to W9 has evolved from the leachate composition in well W1.

2.3. Simulation of transport

A groundwater flow velocity of 4 m/year was assumed as best estimate (Van Breukelen et al., 2003) and used in the model. A time-step of 0.5 years was taken and the cell length was set at 2 m. The flow path was simulated by a series of 80 ‘‘cells’’ with a total length of 160 m (Fig. 1). Since landfilling occurred between 1965 and 1977, and groundwater sampling was performed in the period 1998–1999, duration of advective transport is 34 years at most. Total transport time was optimized using PEST as 30.5 years (see Section 2.6). A flux in the start- and end-cell was taken as boundary condition. The diffusion coefficient was set at 3×10^{-10} m^2/s, while a low value for longitudinal dispersivity of 0.1 m was specified. As the plume length was about 100 m (Fig. 1), a longitudinal dispersivity of 10 m (one tenth of the flow length) could be expected at most (Gelhar, 1986). A longitudinal dispersivity of 10 m could not match constant observed chloride concentrations in the plume, while a value of 1.0 m did not affect results much in comparison with the adopted value of 0.1 m.

2.4. Composition of leachate and pristine groundwater and aquifer geochemistry

Table 1 shows the observed compositions of inflowing leachate and pristine groundwater and the compositions adopted in the model. The composition of pristine ground-

Table 1
Composition of inflowing leachate and pristine groundwater (observed and adopted in model)

Parameter	Unit	Leachate observed[a]	Model	Pristine observed[a]	Model
Chloride	mmol/l	4.03–8.74	7.36	0.34–2.17	1
EC[b]	μS/cm	4520–5260	–	189–754	–
Alkalinity[c]	mmol/l	51.3–56.8	56	0.2–6.6	0.5
pH		6.4–6.7	6.6	4.6–6.7	5
pe[d]		−3.6	−3.6	−2.7 to −3.4	−3.0
Temperature	°C	10–13	11.0	–	11.0
DOC[e]	mmol C/l	8.2–10.3	9.2 (two fractions)	0.25–1.92	0
Oxygen	mmol/l	0	0	0	0
Nitrate[f]	mmol/l	0	0	0 | 1.2 | 6.1	0
Mn(II)	μmol/l	6.4–9.1	–	0.5–13	–
Fe(II)	mmol/l	0.20–1.24	0.81	0.002–0.47	0.11
Sulfate[a]	mmol/l	0.03–0.11	0.06	0.018–1.72	1
Sulfide	μmol/l	3–6	–	0–9	–
Methane	mmol/l	1.33–1.48	1.33	0–0.56	0.1
Nitrogen gas[a]	mmol/l	0.16–0.42	0.28	0.98	0.98
Argon[a]	μmol/l	3.3–7.5	5	16.5	16.5
Ammonium	mmol/l	19.2–19.8	19.8	0.006–0.067	0.067
Calcium	mmol/l	7.83–10.4	10.4	0.42–2.72	0.42
Magnesium	mmol/l	3.1–4.36	3.70	0.12–0.49	0.12
Potassium	mmol/l	5.55–6.14	6.01	0.026–0.41	0.41
Sodium	mmol/l	7.7–9.39	8.22	0.3–2.6	2.6
δ^{13}C-DIC	‰	+13.1	+13.1	−19.55	−19.55
δ^{13}C-CH_4	‰	−53.1	−53.1	−72.6	−72.6
δ^{13}C-DOC	‰	−24 to −30	−27	~ −27	–

[a] Observation well W1b was taken as representative for leachate. For conservative Cl, SO_4, Ar and N_2 observed ranges for the total plume are given. Pristine groundwater was characterized by 13 wells (for Ar and N_2: W8a).

[b] EC = electrical conductivity.

[c] Alkalinity comprises acid buffering of dissolved organic carbon.

[d] pe was calculated from the H_2/H^+ redox couple.

[e] Dissolved organic carbon from the leachate was assumed to be reactive, while pristine DOC was not. In the model, two DOC fractions differing in reactivity were used (see Table 2).

[f] Observed nitrate concentrations in pristine groundwater are given as maximum concentrations for below the plume, above the plume and upstream of the landfill, respectively.

water used in the model was calibrated using PEST (see Section 2.6). The model composition for inflowing leachate was taken equal to the average composition of well W1b, located just below the landfill (Fig. 1). However, for Cl, SO_4, N_2 and Ar, the average concentration observed in the whole plume was adopted, because (near) conservative behaviour is observed. Leachate contains high concentrations of the following species with respect to pristine groundwater: Cl, alkalinity, DOC, Fe(II), CH_4, NH_4, Ca, Mg, K and Na. Leachate leaving the landfill body is supersaturated with respect to siderite and calcite. Concentrations of SO_4, N_2 and Ar are lower in the plume than in pristine groundwater.

The pristine aquifer is anaerobic. Nitrate was observed only in shallow groundwater upstream and above the plume, and was assumed to be absent at plume depth before landfilling started. Nitrate reduction is likely to be an important redox process at the top

fringe of the plume. Van Breukelen et al. (2003) showed that DOC degradation inside the leachate plume was coupled to iron reduction, while sulfate reduction and methanogenesis were restricted to the landfill body. This is reflected by the strong contribution of iron-reducing bacteria of the family *Geobacteraceae* to the microbial communities in this plume (Röling et al., 2001). Iron reduction is expected to be the dominant redox process in the pristine aquifer at plume depth as well. Undersaturation with respect to calcite ($CaCO_3$) and siderite ($FeCO_3$) indicates that the pristine aquifer does not contain these minerals. Supersaturation with respect to siderite and calcite indicates that precipitation of these carbonate minerals probably happens within the leachate plume (Fig. 7).

2.5. Simulation of the biogeochemical processes

2.5.1. Degradation of dissolved organic carbon coupled to reduction of iron oxide

Dissolved organic carbon (DOC) degradation was simulated using first-order kinetics, assuming two DOC fractions differing in reactivity (see Table 2 and Section 3.2). Individual DOC components were not simulated: the total concentration of mono-aromatic hydrocarbons was three orders of magnitude lower than the DOC concentration, while

Table 2
Biogeochemical reactions modelled

Reaction	log*K*[a]	Rate (M/year)	Amount (mmol/l)
Biodegradation DOC			
$DOC \rightarrow CH_2O$		$1.03 \times 10^{-2} \times [DOCp]$[b] $1.06 \times 10^{-1} \times [DOCr]$[b]	6.14 (DOCp) 3.06 (DOCr) 9.2 (total DOC)
$CH_2O + H_2O \rightarrow CO_2 + 4e^- + 4H^+$		instantaneous	
Iron reduction			
$FeOOH + 3H^+ \leftrightarrow Fe^{3+} + 2H_2O$	− 0.15		50
$Fe^{2+} \leftrightarrow Fe^{3+} + e^-$	− 13.02		
Carbonate precipitation			
$CaCO_3 \leftrightarrow Ca^{2+} + CO_3^{2-}$	− 8.48	$7.3 \times 10^{-4} \times (\Omega - 1)$[c]	0
$FeCO_3 \leftrightarrow Fe^{2+} + CO_3^{2-}$	− 10.89	$3.3 \times 10^{-5} \times (\Omega - 1)$[c]	0
Cation exchange and proton buffering			
Cation exchange capacity (CEC)			113 (142 ± 85)[d]
Proton buffer (Y_{tot})			30 (30 ± 24)[d]
Degassing[e]			
$\Sigma p(CO_2, CH_4, Ar, N_2) \leq$ P-hydro		instantaneous	

[a] log*K* is given for 25 °C.

[b] DOCr = reactive fraction of dissolved organic carbon; DOCp = persistent (less reactive) DOC fraction.

[c] Ω = saturation state for specific mineral in groundwater.

[d] CEC (meq/l) = $0.6 \times [\% < 2\ \mu m] \times 10 \times (\rho_b/\varepsilon)$; Y_{tot} (meq/l) = $4.8 \times [\%\ OC] \times 10 \times (\rho_b/\varepsilon)$, (Appelo et al., 1998). For porosity (ε) a value of 0.3 was adopted, while for calculation of the bulk density (ρ_b) the specific weight of quartz (2.65 g/cm^3) was taken for the sediment grains. Model values are given, while observed averages and standard deviations are shown between parenthesis.

[e] P-hydro = hydrostatic pressure = 1.68 atm.

Albrechtsen et al. (1999) measured equally low concentrations of volatile fatty acids in methanogenic-phase leachate under iron-reducing conditions. Dissolved organic carbon in methanogenic-phase leachate consists mainly of humic and fulvic acids (Christensen et al., 1998). Oxidation of soil organic matter was not included because its reactivity was expected to be much lower than the leachate DOC reactivity. Sorption of DOC to sandy aquifer sediments is low (Christensen et al., 2001) and therefore neglected in the model.

Kinetic degradation of DOC was simulated following the two-step partial equilibrium approach (e.g., Brun and Engesgaard, 2002) by transforming conservative (to the model) DOC species into "reactive" CH_2O, which is instantaneously oxidized in the PHREEQC model while maintaining thermodynamic equilibrium. The adopted FeOOH solubility (Table 2) falls in the solubility range for lepidocrocite and was calculated from hydrogen gas concentrations assuming that iron reducers need a minimum threshold of -7 kJ/mol H_2 to oxidize H_2 (Van Breukelen et al., 2003). The hydrogeochemical conditions (absence of oxygen and nitrate, solubility FeOOH, pH) determine that Fe(III) is the preferential electron acceptor and has a higher affinity to accept electrons than sulfate or carbon dioxide. The initial content of FeOOH in the aquifer was taken constant and sufficiently high in order to prohibit depletion of iron oxide close to the landfill.

2.5.2. Precipitation of carbonate minerals

Precipitation of siderite and calcite were modelled as kinetic reactions, because the leachate was supersaturated and far from thermodynamic equilibrium with these mineral phases. Rate of precipitation (R) was modelled as the product of the observed or effective rate constant (k_{obs}) times the saturation state minus 1 (e.g., Nancollas, 1979):

$$R = K_{obs}(\Omega - 1) \tag{1}$$

with

$$\Omega = \frac{IAP}{K} \tag{2}$$

where Ω is the saturation state, IAP is the ion activity product, and K is the thermodynamic equilibrium constant. The saturation state is 1 at thermodynamic equilibrium, and the water is supersaturated with respect to a particular mineral when Ω exceeds 1. The observed rate constants were determined (Table 2) by matching the observed saturation indices of the minerals using PEST (see Section 2.6). The equilibrium constants of calcite and siderite (Table 2) were taken from the PHREEQC database.

2.5.3. Cation exchange and proton buffering

Proton buffering was included in the model because pH changed from slightly acidic in the pristine aquifer to close to neutral in the landfill (Table 1). Proton buffering on soil organic matter (SOM) was modelled according to the approach of Appelo et al. (1998), with exchange coefficients for proton exchange taken from Tipping and Hurley (1992). Proton buffering on iron oxide was neglected because PHREEQC calculations on surface complexation (results not presented) showed that proton desorption from iron oxide was

much less than from SOM. However, it will be of more importance in aquifers having lower SOM to FeOOH ratios.

Following Appelo et al. (1998), cation exchange capacity (CEC) was estimated using the average clay content of the sediments ($3.8 \pm 2.3\%$; $n = 5$), while the amount of proton exchangeable sites (Y_{tot}) was estimated using the average organic carbon content of the aquifer ($0.10 \pm 0.08\%$; $n = 5$; Table 2). Exchange coefficients on clay and organic matter were taken from the PHREEQC database and Appelo et al. (1998), respectively. Exchange coefficients of $Fe^{2+}$and NH_4^+ to organic matter are not known, but were assumed to be equal to Mg^{2+} (Griffioen, 1992) and K^+ (Bruggenwert and Kamphorst, 1982), respectively. The exchange coefficient of Fe^{2+} to clay (X^-) was taken equal to Mg^{2+}.

2.5.4. Degassing

The landfill leachate plume contains high concentrations of CH_4 and CO_2, and the total gas pressure exceeds hydrostatic pressure (Van Breukelen et al., 2003). Gas bubbles may therefore form (Blicher-Mathiesen et al., 1998), and volatilization from the plume may occur. In particular, volatile methane can be expected to decrease in concentration as a result of degassing (Baedecker et al., 1993).

PHREEQC calculates, given the hydrostatic pressure, whether or not a gas phase forms including the moles of gas and its composition in equilibrium with groundwater. Gases included in the model were: CO_2, CH_4, N_2 and Ar. The hydrostatic pressure was fixed at 1.68 atm along the flow path, which was in the range of hydrostatic pressure along the flow path (1.5 to 1.7 atm), and equal to the total gas pressure of the leachate source composition. A developing gas phase was modelled to be instantaneously lost from the leachate.

2.5.5. Modelling of ^{13}C isotope geochemistry

The carbon isotope geochemistry was simulated in PHREEQC by adding "C12" and "C13" as separate imaginary solutes to the model. The exact concentration of ^{12}C and ^{13}C was calculated from the DIC isotope signature in leachate and pristine groundwater (Table 1). Degradation of DOC was simulated without isotope fractionation, and C12 and C13 were added to the model cells in absolute amounts calculated from the average observed $\delta^{13}C$-DOC value of $-27‰$ (Van Breukelen et al., 2003).

Potential anaerobic methane oxidation was simulated as a first-order process, and fractionation as a result of oxidation was included:

$$R^{13}C = k[CH_4]\left(\frac{[^{13}C]}{[^{13}C]+[^{12}C]}\right) \quad (1)$$

and

$$R^{12}C = k[CH_4]\left(\frac{[^{12}C]}{[^{13}C]+[^{12}C]}\right)\alpha \quad (2)$$

where $R^{13}C$ and $R^{12}C$ are the oxidation rates of ^{13}C-CH_4 and ^{12}C-CH_4, respectively, k is the rate constant for methane oxidation fitted to the observed downstream methane decrease, $[i]$ is concentration of species i, and α is the fractionation factor ($\alpha = 1.014$).

This value has been calculated for anaerobic methane oxidation observed within another landfill leachate plume (Grossman et al., 2002). The δ^{13}C-CH_4 of inflowing leachate and pristine groundwater was taken at -53.1‰ and -72.6‰, respectively (Table 2).

The δ^{13}C of precipitating carbonate minerals (siderite and calcite) was determined at each time step and distance by calculating the δ^{13}C of bicarbonate (using [HCO_3^-], [CO_2], δ^{13}C-DIC and a fractionation factor $^{13}\varepsilon_{\text{bicarbonate}-CO_2(aq)}$ of $+10.6$‰ (Mook, 2000)) and adopting a fractionation factor ($^{13}\varepsilon_{\text{carbonate mineral}-\text{bicarbonate}}$) relative to bicarbonate. Two sets of fractionation factors ($^{13}\varepsilon_{\text{carbonate mineral}-\text{bicarbonate}}$) were tested (see Section 3).

Finally, the effect of carbon dioxide degassing on δ^{13}C-DIC was simulated. Following the approach of carbonate mineral precipitation, δ^{13}C-CO_2(g) was calculated using δ^{13}C-CO_2 (aq) and taking a fractionation factor $^{13}\varepsilon_{CO_2(g)-CO_2(aq)}$ of $+1.13$‰ at 11 °C (Mook, 2000).

2.6. Calibration of the reactive transport model using PEST

Calibration of the model was done using the parameter estimation software PEST (Watermark Numerical Computing, http://www.sspa.com/pest). PEST optimizes the sum of weighted least squares between the model outputs and the field observations by changing assigned model parameters within given ranges of uncertainty. The program uses a nonlinear estimation technique known as the Gauss–Marquardt–Levenberg method.

The following model parameters were optimized: Fe(II), Ca, Mg, K, Na and NH_4 of pristine groundwater (within observed concentration range), observed rate constant (k_{obs}) for siderite and calcite precipitation, oxidation rate of the two DOC fractions (rate of reactive fraction was set 10 times faster than less reactive fraction), proportion of the two DOC fractions, total transport time, and cation exchange capacity (CEC). Cation exchange capacity was optimized because the standard deviation of the estimates was high. The optimum found was 20% less than the calculated average (see Section 2.5.3 and Table 2). Other parameters were kept constant.

The following groundwater hydrochemical variables were used as constraints and taken to calculate the weighted sum of square differences with model results: pH, DIC, DOC, Na, K, Ca, Mg, NH_4, Fe(II), together with the saturation indices of siderite and calcite (for SI calcite only well W2b was used because SI>0 at that point). Eight screens were used (W2b–W9b), and for each screen average values over time ($n=3$) were taken. Consequently, the total sum consisted of 81 square differences.

The weight factor for each variable was taken as the reciprocal of its average observed concentration in the plume. High sum of residuals for cations (NH_4>Ca>K>Mg ≈ Fe(II)) resulted in a suboptimal fit for variables having a low sum of residuals. Therefore, weight factors of some key variables were multiplied to enhance the fit: pH ($\times 10$), DOC ($\times 10$), SI siderite and SI calcite ($\times 10^{1/2}$).

3. Results of reactive transport modelling

Several reactive transport simulations (S1–S8) will be discussed (see Table 3) to show the effects of the various processes on the downstream change in leachate composition.

Table 3

Simulation	Processes included	Remarks
S1	No reactions (only conservative transport)	
S2	Cation exchange and proton buffering	
S3	S2 + DOC degradation coupled to iron reduction	
S4	S3 + methane oxidation coupled to iron reduction	
S5	S3 + precipitation of siderite and calcite	Fe(II) pristine = min. observed
S6	Idem	Fe(II) pristine = calibrated
	S6a: $^{13}\varepsilon_{calcite-bicarbonate}$, $^{13}\varepsilon_{siderite-bicarbonate} = 0.21$ ‰	
	S6b: $^{13}\varepsilon_{calcite-bicarbonate} = 1$ ‰ , $^{13}\varepsilon_{siderite-bicarbonate} = 2.7$ ‰	
S7	S6 + degassing	Complete and calibrated model
S8	S7, but without proton buffering	

3.1. Cation exchange and proton buffering

Cation exchange and proton buffering change the composition of the leachate flowing through the aquifer. Fig. 2 shows the composition of the total exchanger ($T = \Sigma X + Y_{tot}$) along the flow path for the final model (S7). Exchangeable (i.e., sorbed on the exchanger) ammonium and potassium increased, while exchangeable calcium and Fe(II) decreased in the first 60 m of the flow path with respect to pristine groundwater further downstream. Potassium and ammonium retard due to cation exchange at clay minerals with mainly Ca and Fe(II). Exchangeable Fe(II) is thus released to the leachate. Fig. 2 shows that proton buffering causes desorption of protons from sedimentary organic carbon, in response to an increase in pH by inflow of leachate. Proton buffering causes about a unit of decrease in pH at the front of the plume (compare simulation S7 with S8 in Fig. 8), and subsequently may trigger degassing (see Section 3.4) as bicarbonate shifts to carbon dioxide (Fig. 9).

The fit of sodium observations is fair, and for potassium and magnesium reasonable (Figs. 3 and 4). However, simulated calcium and ammonium concentrations further than 50 m downstream were higher and much lower, respectively, than observed (Figs. 3 and 4). PEST used the maximum observed pristine concentrations of K, Na, and NH_4, and the minimum observed concentration of Ca in order to suppress simulated concentrations of calcium and

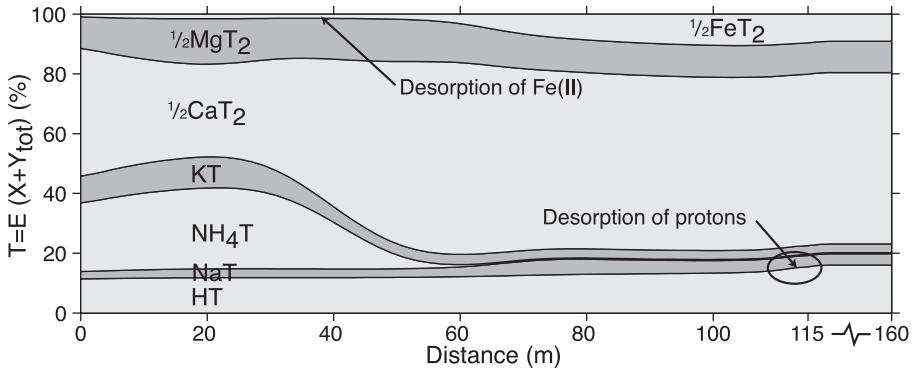

Fig. 2. Simulation of exchange site composition ($T = \Sigma(X + Y_{tot})$) along the flow path.

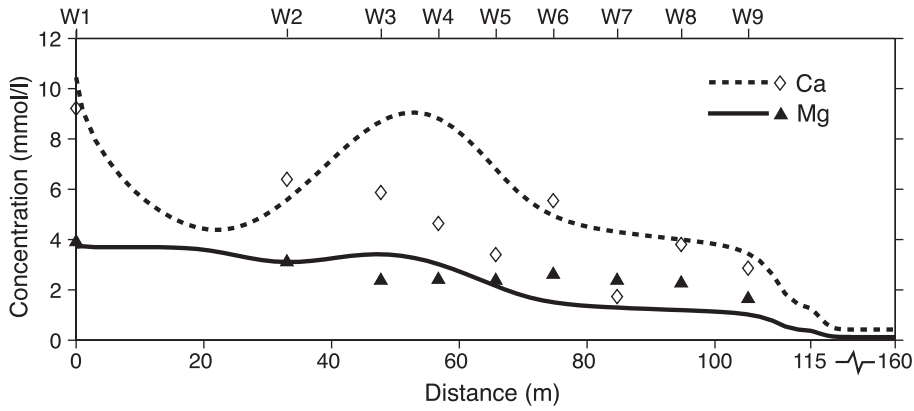

Fig. 3. Observations and simulation of calcium (◇) and magnesium (▲).

improve the overall fit of the model. Varying the exchange selectivity coefficients of Ca and NH_4 within reported ranges (Bruggenwert and Kamphorst, 1982) did not significantly improve the fit of Ca (results not shown). Excluding proton buffering from the model slightly decreased the match with Fe(II) and Ca observations (results not shown). Retardation factors for potassium and ammonium were calculated as, respectively, 3.4 and 2.9 using model concentrations, but for ammonium observed retardation seems less than 2.

3.2. Degradation of dissolved organic carbon coupled to iron reduction

Degradation of DOC is coupled to reduction of iron oxide in the leachate plume (Van Breukelen et al., 2003). Zero- or first-order DOC degradation kinetics did not result in a reasonable match with observations (results not shown), as a consequence of a very sluggish decrease of observed DOC concentration in the downstream part of the plume (Fig. 5). Monod kinetics may be a suitable rate formulation but describes biodegradation

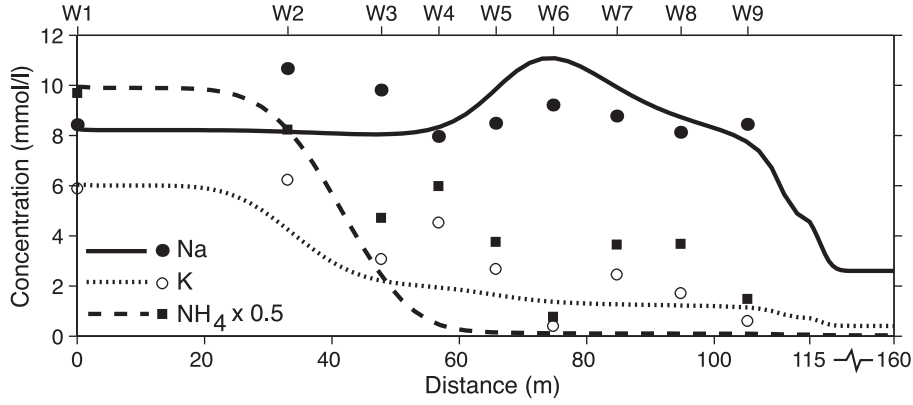

Fig. 4. Observations and simulation of sodium (●), potassium (○) and ammonium (■).

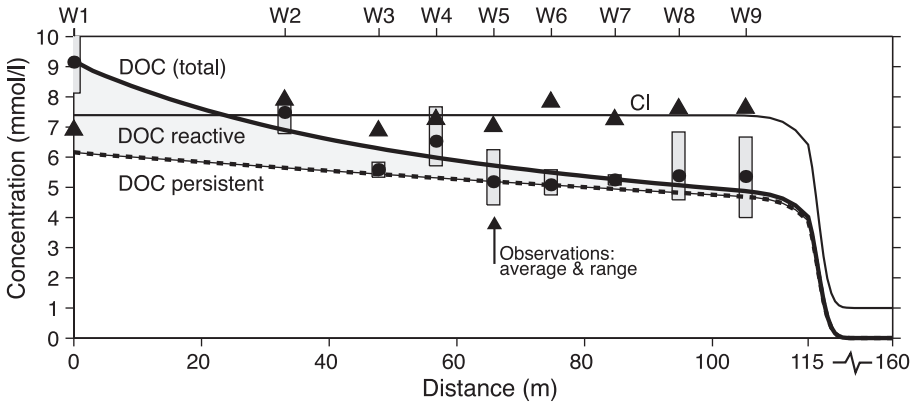

Fig. 5. Observations and simulation of dissolved organic carbon (●) and chloride (▲).

of specific substrates and consequently does not apply for leachate DOC. Biodegradation of complex organic matter like DOC is usually simulated considering an infinite number of reactive fractions (Bosatta and Ågren, 1995). Here, a simpler model considering first-order degradation of only two DOC fractions with different reactivity simulated observations well (Table 2, Fig. 5). The decrease in overall DOC reactivity downstream is caused by depletion of the reactive DOC fraction according to this degradation model. PEST optimized the proportion of the most reactive fraction as a third of total DOC.

The content of iron oxide was almost completely consumed close to the landfill after 30.5 years (Fig. 6). However, the few measurements do not show a decrease in iron oxide content towards the landfill. Depletion of iron oxide downstream from the landfill is however expected in the near future as degradation proceeds. Taking a lower solubility for FeOOH equal to goethite ($\log K = -1.0$) causes iron reduction to be energetically less favorable and results in a short sulfate-reducing zone at the landfill border succeeded by simultaneous methanogenesis and iron reduction downstream (Fig. 11). FeS was allowed to precipitate in this model. Note that, once methanogenesis is active, degassing strongly

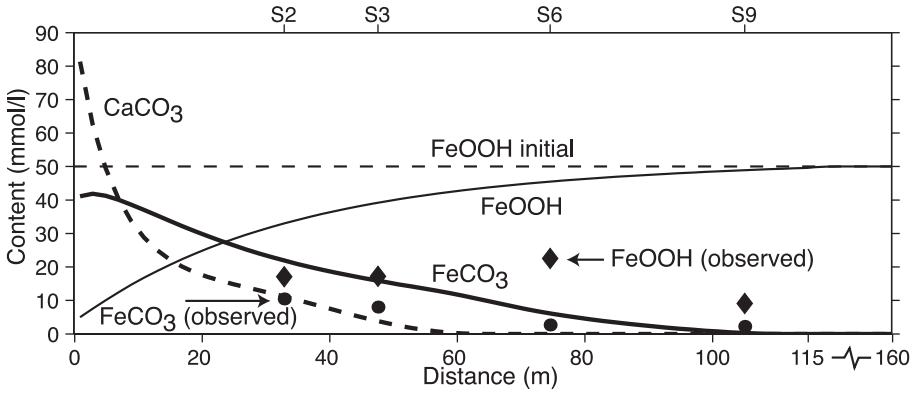

Fig. 6. Observations and simulation of iron oxide, siderite, and calcite content.

impedes the methane concentration to increase downstream. This illustrates that occurrence of methanogenesis is difficult to determine from methane concentrations in contaminant plumes, once the sum of partial gas pressures starts to exceed the hydrostatic pressure.

Simulation S3 indicates that, if only cation exchange and iron reduction would occur, pH, DIC and Fe(II) should increase downstream (Figs. 8–10). However, decreases in pH and DIC were observed, while the observed dissolved Fe(II) concentrations were much lower than the calculated Fe(II) concentrations (up to 14 mmol/l), resulting in simulated saturation indices of siderite (up to 3.5) and calcite (up to 2.0) which are much higher than observations (results not shown).

3.3. Precipitation of calcite and siderite

The discrepancy between field observations and model S3, which excludes precipitation of carbonate minerals, indicates that precipitation of siderite ($FeCO_3$) and calcite ($CaCO_3$) takes place. Kinetic precipitation was simulated because observed saturation indices for these minerals were substantially above zero (siderite: 0.8–1.8, calcite up to 0.8 near the landfill).

Rate constants for calcite and siderite precipitation were obtained by calibration using PEST and are shown in Table 2. One should note that the rate constant depends on the solubility constant of siderite, because the saturation state depends on this constant. The reported range of the thermodynamic equilibrium constant for siderite varies from -10.45 to -11.20 (Jensen et al., 2002) and our adopted value (-10.89) fits in this range. The calibrated rate constant for siderite precipitation (3.3×10^{-5} mol/l/year) is about 20 times lower than for calcite (7.3×10^{-4} mol/l/year). However, absolute amounts of precipitated calcite and siderite are about equal (Fig. 6), as the lower rate constant is compensated by the higher saturation state of siderite. Lower rate constants for iron carbonate with respect to calcium carbonate precipitation, have generally been observed (Wajon et al., 1985; Jensen et al., 2002). Halving or doubling of the calibrated rate constant resulted in upper and lower limits of observed SIs for siderite (Fig. 7). Observed rate constants for both

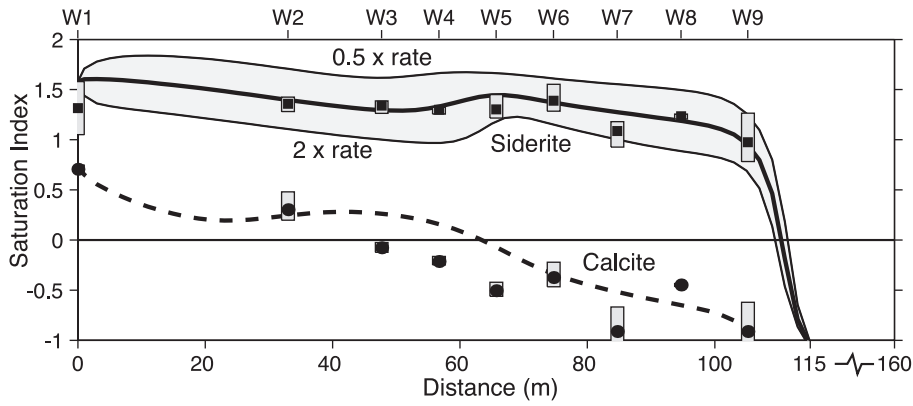

Fig. 7. Observations and simulation of saturation indices (SIs) of siderite (■) and calcite (●). Simulated SIs of siderite are also shown using the halved or doubled calibrated rate constant.

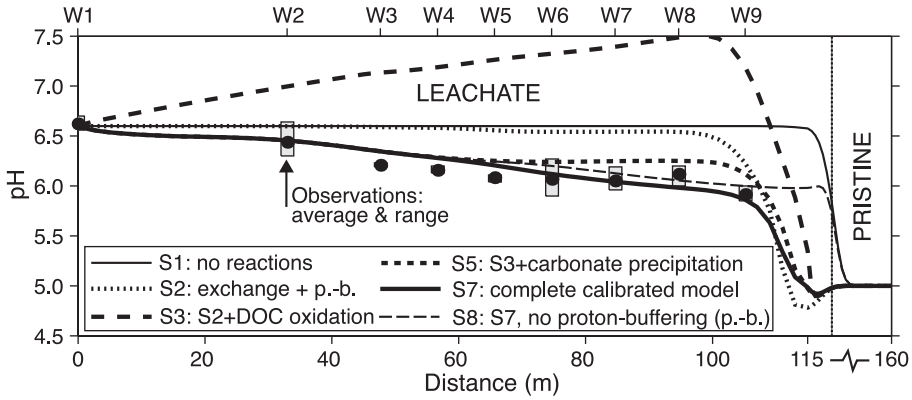

Fig. 8. Observations and simulations of pH.

siderite and calcite precipitation are low in comparison with reported values and are attributed to the initial absence of these minerals in the aquifer and the presence of fulvic acids in leachate, and to less extent to the low temperature of groundwater (Van Breukelen, 2003).

The final model (S7) calculates a maximum of 120 mmol/l of carbonate minerals precipitated at the landfill border (Fig. 6), which corresponds to a carbonate fraction of 0.023% C at a porosity of 0.3. This amount is much smaller than the detection limit of the measurement method used (0.5% C). Therefore, direct observational proof for precipitation of carbonate minerals was not acquired. Observations for siderite plotted in Fig. 6 are semiquantitative measurements based on chemical extractions and are indicative of the total amount of siderite present (Van Breukelen et al., 2003).

Precipitation of siderite and calcite decreases pH and DIC in downstream direction in agreement with the observations (Figs. 8 and 9). The SIs for siderite and calcite were also well matched by the model (Fig. 7). An important model variable was the adopted concentration of Fe(II) in pristine groundwater. PEST optimized the Fe(II) concentration

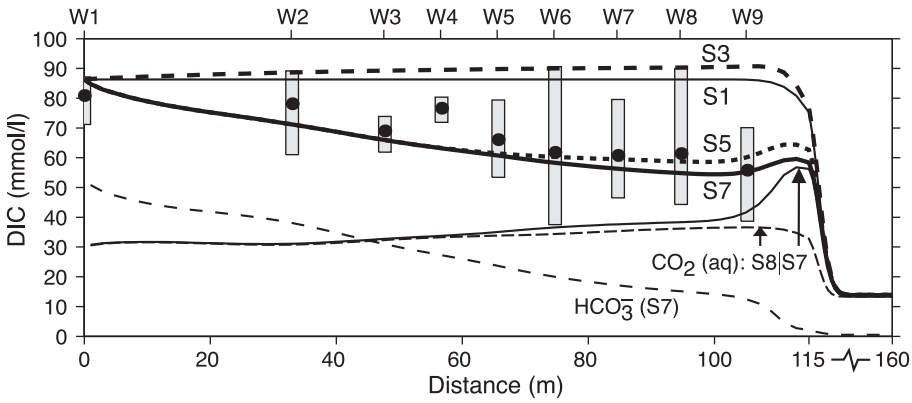

Fig. 9. Observations and simulations of dissolved inorganic carbon (DIC).

(0.11 mmol/l) close to the observed average in pristine groundwater (0.12 ± 0.12 mmol/l, $n = 26$). A higher Fe(II) concentration at pristine conditions leads to a higher Fe-occupancy of the exchanger at pristine conditions. This implies a larger amount of Fe(II) expelled due to cation exchange, when NH_4-rich leachate enters the aquifer, and siderite precipitation is initiated upon pH increase. Therefore, Fe(II) at pristine conditions together with the rate constant for DOC degradation mainly control the amount of siderite precipitated, and consequently the DIC concentration. For example, if the minimum observed Fe(II) concentration was adopted (~ 2 μmol/l), Fe(II) released due to cation exchange was substantially lower (simulation S5). Consequently, simulated Fe(II) was lower than observed (Fig. 10), less siderite was precipitated (result not shown) and pH simulated in the front part of the plume was too high (Fig. 8).

3.4. Degassing

Fig. 12 shows the simulated partial gas pressures of CO_2, CH_4, N_2 and Ar for the final model, as well as the total gas pressure for the simulation excluding degassing (S5). The gas pressure in the leachate is high due to production of CO_2 and CH_4 inside the landfill body. The total gas pressure starts to exceed the hydrostatic pressure from about 40 m downstream in case degassing is not simulated (S5). It reaches a maximum pressure (2.2 atm) at the front of the plume. Carbon dioxide and methane are lost in about equal molar amounts when degassing is modelled (i.e., total gas pressure is not allowed to exceed hydrostatic pressure). However, the relative loss of methane is much higher, due to its lower solubility. The simulated decrease in methane by degassing at the most downstream well W9b was 14%, while a decrease of 34% was observed (Fig. 11). Mono-aromatic pollutants will not be attenuated by degassing as these compounds are much less volatile than methane.

Degassing is not likely to be caused by in situ production of gases in this aquifer (DIC production due to DOC oxidation is less than DIC removal by precipitation of carbonate minerals), but is triggered in our case by both proton buffering and precipitation of

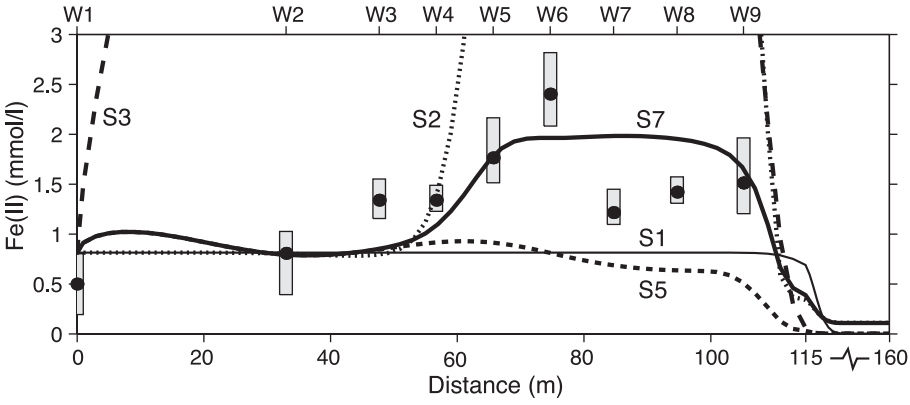

Fig. 10. Observations and simulations of Fe(II).

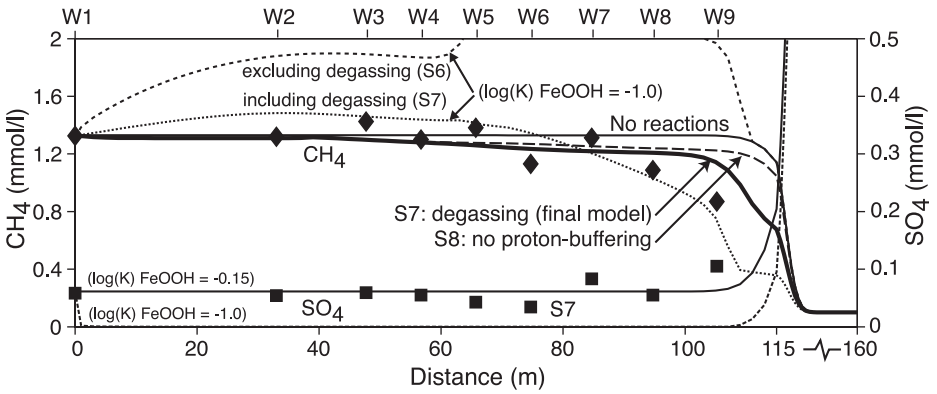

Fig. 11. Observations and simulations of dissolved methane (♦) and sulfate (■).

carbonate minerals. Both geochemical processes cause a decrease in leachate pH (Fig. 8), which shifts bicarbonate to carbon dioxide (Fig. 9) and consequently increases pCO_2 and total gas pressure (Fig. 12). Carbonate mineral precipitation induces degassing between 40 and 100 m downstream, while proton buffering is the main trigger at the front part of the plume (Fig. 11).

3.5. Modelling the carbon isotope geochemistry of the leachate plume

Simulation of δ^{13}C-DIC was performed to verify the model. Fig. 13 presents the contribution of various processes to the δ^{13}C-DIC evolution. Oxidation of DOC contributes inorganic carbon depleted in δ^{13}C (-27‰) and consequently lowers δ^{13}C-DIC in the direction of flow (Fig. 13: S3). The observed δ^{13}C-DIC decrease; however, is larger and supports occurrence of carbonate mineral precipitation (Fig. 13: S6a, S6b). Carbonate mineral precipitation and DOC oxidation have a comparable impact on the δ^{13}C-DIC decrease.

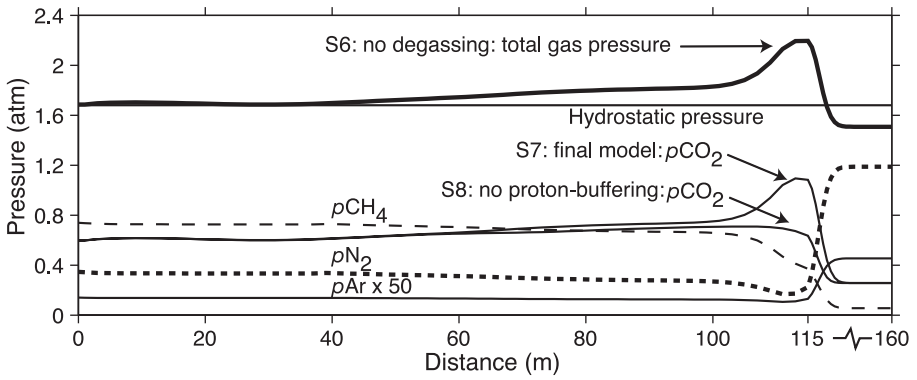

Fig. 12. Simulation of degassing of dissolved gasses in leachate plume.

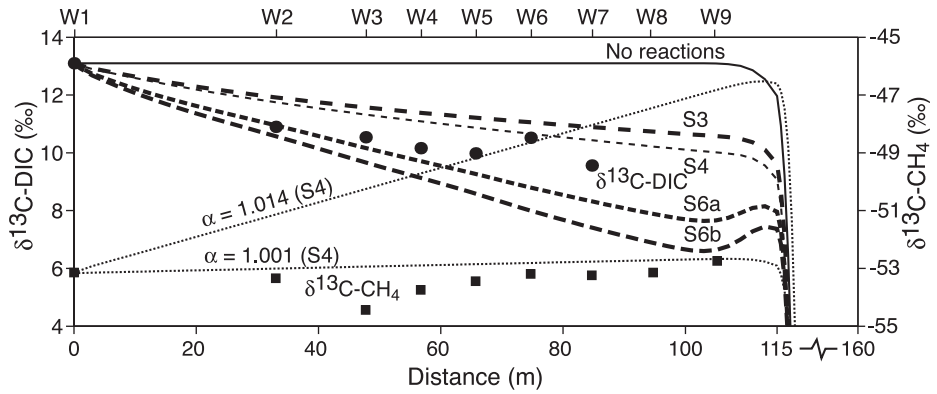

Fig. 13. Observations and simulations of the carbon isotope geochemistry: δ^{13}C-DIC (●) and δ^{13}C-CH_4 (■). Results are shown for DOC oxidation (S3) in combination with anaerobic methane oxidation (S4) or precipitation of carbonate minerals (S6a and S6b).

The fractionation factor for calcite precipitation differs somewhat in literature, and has not been determined for siderite precipitation at low temperature. Simulations were therefore run with two sets of fractionation factors (Table 3: S6a and S6b). For simulation S6a, the fractionation factor for $CaCO_3$ at a temperature of 11 °C (+0.21‰) was taken from Mook (2000) and was assumed to apply for $FeCO_3$ as well. Romanek et al. (1992) observed higher fractionation factors for calcite and aragonite: +1.0‰ and +2.7‰, respectively. Fractionation of aragonite conducted in experiments between 10 and 40 °C (Romanek et al., 1992) appeared similar to carbon-13 fractionation of siderite measured recently in precipitation experiments between 45 and 75 °C (Zhang et al., 2001). The fractionation factor for siderite can therefore be taken from aragonite for this low-temperature aquifer (Horita and Zhang, personal communication). Simulation S6b adopted the higher fractionation factors observed by Romanek et al. (1992) and therefore resulted in a stronger δ^{13}C-DIC decrease. Simulation S6a simulated observations closer than simulation S6b (Fig. 13).

The effect of carbonate mineral precipitation on the downstream δ^{13}C-DIC decrease is considerable because of the slightly acidic conditions in this aquifer. The positive equilibrium fractionation factors between DIC species and carbonate minerals results in a preferential removal of ^{13}C from the leachate. However, the equilibrium fractionation factor with respect to carbonate minerals is much higher for dissolved carbon dioxide than for bicarbonate ($^{13}\varepsilon_{\text{bicarbonate}-CO_2}$(aq) ~ +9.5‰ at 20 °C and +11.4‰ at 5 °C (Mook, 2000)). Therefore, fractionation due to carbonate mineral precipitation is relatively large under the slightly acidic conditions in this aquifer, where $CO_{2(aq)}$ makes up a large part of DIC, compared to fractionation at neutral and alkaline pH, where bicarbonate or carbonate dominate DIC.

Degassing of carbon dioxide from the plume had a negligible effect on δ^{13}C-DIC, because the amount of degassed CO_2 was low with respect to total DIC (results of simulation not shown). The potential effect of anaerobic methane oxidation on δ^{13}C-DIC was little compared to DOC oxidation or carbonate mineral precipitation (Fig. 13). In

disagreement with observations, the model predicts a strong increase in δ^{13}C-CH_4 values downstream (Fig. 13). A much lower fractionation factor ($\alpha = 1.001$) below the reported range for oxidation ($\alpha = 1.003 - 1.037$) but indicative for degassing (Bergamaschi, 1997) explained observations better. Consequently, occurrence of anaerobic methane oxidation in this plume is unlikely, which confirms an earlier interpretation (Van Breukelen et al., 2003). Simulation of the carbon isotope geochemistry supports the probability of the hydrogeochemical model, and indicates that carbonate mineral precipitation occurs, although δ^{13}C-DIC observations were not perfectly matched.

4. Discussion and conclusion

Multicomponent geochemical transport modelling was used to obtain quantitative insight into the reactions contributing to the changes in leachate composition downstream of the Banisveld landfill, the Netherlands. A combination of reactions needed to be incorporated in the model in order to simulate observations: degradation of DOC coupled to reduction of iron oxide, cation exchange, proton buffering, and kinetic precipitation of siderite and calcite. Degassing provides an explanation for downstream decreasing methane concentrations and was triggered at the site studied by carbonate mineral precipitation and proton buffering both increasing pCO_2 by decreasing the pH. Remarkably, it was sufficient to adopt a constant leachate composition, while in other studies spatial heterogeneity (Brun et al., 2002) or temporal variability of the source (Van Breukelen et al., 1998) had to be accounted for. Simulation of the carbon isotope geochemistry confirmed the proposed reaction network independently. The study demonstrated the relevance and impact of various secondary geochemical processes on leachate plume evolution. However, the approach of modelling the processes is nonunique. For example, proton buffering on iron oxide was omitted, a different rate law for degradation could have been adopted (e.g., taking the content of iron oxide as additional parameter (Liu et al., 2001), Monod kinetics with microbial growth), precipitation of solid solutions may have happened, and the surface area could have been incorporated in the rate formulation for mineral precipitation.

This and other studies (Baedecker et al., 1993; Revesz et al., 1995) indicate that degassing is an essential secondary process to consider in solving the reaction network controlling methane. Methanogenesis will be underestimated for gas-saturated plumes if the occurrence of gas exsolution is not accounted for (see Fig. 11). The significance of secondary methane-oxidizing redox reactions at the fringe of pollution plumes, as demonstrated by Hunter et al. (1998) via reactive transport modelling, will increase substantially if degassing is considered. Furthermore, degassing can lead to formation of a separate gas phase in aquifer pores and may reduce the permeability of an aquifer. The flow direction and/or velocity may change as a result (Ronen et al., 1989; Yager and Fountain, 2001). This might also be an explanation for local water table mounds observed at landfill sites (Christensen et al., 2001).

The various secondary geochemical processes identified in this specific plume should be considered as being of general importance for landfill leachate plume evolution. Cation exchange will manifest since leachate generally contains a different salt composition and

higher salt concentration than fresh groundwater in pristine aquifers (Bjerg et al., 1993; Griffioen, 1999). Cation exchange buffers Fe(II) and retards K^+ and NH_4. Proton buffering should be considered because pH changes in these systems can be considerable (Griffioen, 1999). Cation exchange and iron reduction contribute to the supersaturation of leachate with respect to Ca- and Fe-carbonates, respectively, and this shows that precipitation is kinetically controlled. Finally, high production of CH_4 and CO_2 in the landfill body and plume makes the necessity to consider degassing evident.

Simulations indicate that the rate of siderite precipitation equals or exceeds the rate of iron reduction. Cation exchange buffers released Fe(II) as well. Using the aqueous Fe(II) concentration to quantify iron reduction (Wiedemeier et al., 1995) will therefore result in underestimating the extent of reductive dissolution of Fe-oxides, and associated extent of organic species degradation. A multiple solute model is not able to simulate siderite precipitation or other geochemical reactions, and could therefore only match dissolved Fe(II) in an aromatic hydrocarbon plume when the stoichiometry ratio of Fe(II) released per amount of Fe(III) reduced was adjusted from 1 to 1 down to 0.18 to 1 (Essaid et al., 1995). Geochemical-based reactive transport models can account for secondary geochemical reactions and hold therefore more promise for simulating the evolution of pollution plumes.

Acknowledgements

We thank C. Anthony J. Appelo for correcting the PHREEQC-2 code on calculation of kinetics in the first cell of a transport model. The error has been removed in version 2.4. The two anonymous reviewers are thanked for their comments, which improved the quality of this article.

References

Abrams, R.H., Loague, K., 2000a. A compartmentalized solute transport model for redox zones in contaminated aquifers: 1. Theory and development. Water Resour. Res. 36 (8), 2001–2013.

Abrams, R.H., Loague, K., 2000b. A compartmentalized solute transport model for redox zones in contaminated aquifers: 2. Field-scale simulations. Water Resour. Res. 36 (8), 2015–2029.

Albrechtsen, H.-J., Bjerg, P.L., Ludvigsen, L., Rügge, K., Christensen, T.H., 1999. An anaerobic field injection experiment in a landfill leachate plume, Grindsted, Denmark: 2. Deduction of anaerobic (methanogenic, sulfate-, and Fe(III)-reducing) redox conditions. Water Resour. Res. 35 (4), 1247–1256.

Andrews, J.N., 1992. Mechanisms for noble gas dissolution by groundwaters. Isotopes of Noble Gases as Tracers in Environmental Studies. IAEA, Vienna, pp. 87–110.

Appelo, C.A.J., Verweij, E., Schäfer, H., 1998. A hydrogeochemical transport model for an oxidation experiment with pyrite/calcite/exchangers/organic matter containing sand. Appl. Geochem. 13 (2), 257–268.

Baedecker, M.J., Cozzarelli, I.M., Eganhouse, R.P., Siegel, D.I., Bennett, P.C., 1993. Crude oil in a shallow sand and gravel aquifer: III. Biogeochemical reactions and mass balance modeling in anoxic groundwater. Appl. Geochem 8 (6), 569–586.

Bergamaschi, P., 1997. Seasonal variations of stable hydrogen and carbon isotope ratios in methane from a Chinese rice paddy. J. Geophys. Res.-Atmos 102 (D21), 25383–25393.

Bjerg, P.L., Ammentorp, H.C., Christensen, T.H., 1993. Model simulations of a field experiment on cation exchange-affected multicomponent solute transport in a sandy aquifer. J. Contam. Hydrol. 12 (4), 291–311.

Blicher-Mathiesen, G., McCarty, G.W., Nielsen, L.P., 1998. Denitrification and degassing in groundwater estimated from dissolved dinitrogen and argon. J. Hydrol. 208 (1–2), 16–24.

Bosatta, E., Ågren, G.I., 1995. The power and reactive continuum models as particular cases of the Q-theory of organic-matter dynamics. Geochim. Cosmochim. Acta 59 (18), 3833–3835.

Bruggenwert, M.G.M., Kamphorst, A., 1982. Survey of experimental information on cation exchange in soil systems. In: Bolt, G.H. (Ed.), Soil Chemistry B. Physico-Chemical Models. Elsevier, Amsterdam, pp. 141–204.

Brun, A., Engesgaard, P., 2002. Modelling of transport and biogeochemical processes in pollution plumes: literature review and model development. J. Hydrol. 256 (3–4), 211–227.

Brun, A., Engesgaard, P., Christensen, T.H., Rosbjerg, D., 2002. Modelling of transport and biogeochemical processes in pollution plumes: Vejen landfill, Denmark. J. Hydrol. 256 (3–4), 228–247.

Christensen, J.B., Jensen, D.L., Grøn, C., Filip, Z., Christensen, T.H., 1998. Characterisation of the dissolved organic carbon in landfill leachate polluted groundwater. Water Res. 32 (1), 125–135.

Christensen, T.H., Bjerg, P.L., Banwart, S.A., Jakobsen, R., Heron, G., Albrechtsen, H.-J., 2000. Characterization of redox conditions in groundwater contaminant plumes. J. Contam. Hydrol. 45 (3–4), 165–241.

Christensen, T.H., Kjeldsen, P., Bjerg, P.L., Jensen, D.L., Christensen, J.B., Baun, A., Albrechtsen, H.J., Heron, C., 2001. Biogeochemistry of landfill leachate plumes. Appl. Geochem. 16 (7–8), 659–718.

Clement, T.P., Sun, Y., Hooker, B.S., Petersen, J.N., 1998. Modeling multispecies reactive transport in ground water. Ground Water Monit. Remediat. 18 (2), 79–92.

Essaid, H.I., Bekins, B.A., Godsy, E.M., Warren, E., Baedecker, M.J., Cozzarelli, I.M., 1995. Simulation of aerobic and anaerobic biodegradation processes at a crude oil spill site. Water Resour. Res. 31 (12), 3309–3327.

Gelhar, L.W., 1986. Stochastic subsurface hydrology from theory to applications. Water Resour. Res. 22 (9), 135S–145S.

Griffioen, J., 1992. Cation-exchange and carbonate chemistry in aquifers following groundwater flow. PhD thesis, Vrije Universiteit, Amsterdam. 182 pp.

Griffioen, J., 1999. Comment on 'Kinetic modelling of microbially-driven redox chemistry of subsurface environments: Coupling transport, microbial metabolism and geochemistry' by K.S. Hunter, Y. Wang and P. Van Cappellen. .J. Hydrol. 226 (1–2), 121–124.

Grossman, E.L., Cifuentes, L.A., Cozzarelli, I.M., 2002. Anaerobic methane oxidation in a landfill-leachate plume. Environ. Sci. Technol. 36 (11), 2436–2442.

Hunter, K.S., Wang, Y., Van Cappellen, P., 1998. Kinetic modeling of microbially-driven redox chemistry of subsurface environments: coupling transport, microbial metabolism and geochemistry. J. Hydrol. 209, 56–80.

Islam, J., Singhal, N., O'Sullivan, M., 2001. Modeling biogeochemical processes in leachate-contaminated soils: a review. Transp. Porous Media 43 (3), 407–440.

Jensen, D.L., Boddum, J.K., Tjell, J.C., Christensen, T.H., 2002. The solubility of rhodochrosite ($MnCO_3$) and siderite ($FeCO_3$) in anaerobic aquatic environments. Appl. Geochem. 17 (4), 503–511.

Keating, E.H., Bahr, J.M., 1998. Reactive transport modeling of redox geochemistry: approaches to chemical disequilibrium and reaction rate estimation at a site in northern Wisconsin. Water Resour. Res. 34 (12), 3573–3584.

Krumholz, L.R., Caldwell, M.E., Suflita, J.M., 1996. Biodegradation of 'BTEX' hydrocarbons under anaerobic conditions. In: Crawford, R.L., Crawford, D.L. (Eds.), Bioremediation: Principles and Applications. Cambridge Univ. Press, UK, pp. 61–99.

Liu, C.X., Kota, S., Zachara, J.M., Fredrickson, J.K., Brinkman, C.K., 2001. Kinetic analysis of the bacterial reduction of goethite. Environ. Sci. Technol. 35 (12), 2482–2490.

Mayer, K.U., Benner, S.G., Frind, E.O., Thornton, S.F., Lerner, D.N., 2001. Reactive transport modeling of processes controlling the distribution and natural attenuation of phenolic compounds in a deep sandstone aquifer. J. Contam. Hydrol. 53 (3–4), 341–368.

Mook, W.G., 2000. Environmental isotopes in the hydrological cycle. Principles and applications. Volume I. Introduction: Theory, Methods, Review. UNESCO/IAEA, Vienna. 280 pp.

Murphy, E.M., Ginn, T.R., 2000. Modeling microbial processes in porous media. Hydrogeol. J. 8 (1), 142–158.

Nancollas, G.H., 1979. The growth of crystals in solution. Adv. Colloid Interface Sci. 10, 215–252.

Parkhurst, D.L., Appelo, C.A.J., 1999. User's guide to PHREEQC (version 2)—a computer program for speci-

ation, batch-reaction, one-dimensional transport, and inverse geochemical calculations. Water-Resources Investigations Report 99-4259, U.S. Geol. Survey.

Prommer, H., Davis, G.B., Barry, D.A., 1999. Geochemical changes during biodegradation of petroleum hydrocarbons: field investigations and biogeochemical modelling. Org. Geochem. 30 (6), 423–435.

Revesz, K., Coplen, T.B., Baedecker, M.J., Glynn, P.D., Hult, M., 1995. Methane production and consumption monitored by stable H and C isotope ratios at a crude oil spill site, Bemidji, Minnesota. Appl. Geochem. 10 (5), 505–516.

Röling, W.F.M., Van Breukelen, B.M., Braster, M., Lin, B., Van Verseveld, H.W., 2001. Relationships between microbial community structure and hydrochemistry in a landfill leachate-polluted aquifer. Appl. Environ. Microbiol. 67 (10), 4619–4629.

Romanek, C.S., Grossman, E.L., Morse, J.W., 1992. Carbon isotopic fractionation in synthetic aragonite and calcite—effects of temperature and precipitation rate. Geochim. Cosmochim. Acta 56 (1), 419–430.

Ronen, D., Berkowitz, B., Magaritz, M., 1989. The development and influence of gas-bubbles in phreatic aquifers under natural flow conditions. Transp. Porous Media 4 (3), 295–306.

Tipping, E., Hurley, M.A., 1992. A unifying model of cation binding by humic substances. Geochim. Cosmochim. Acta 56 (10), 3627–3641.

Van Breukelen, B.M., 2003. Natural attenuation of landfill leachate: a combined biogeochemical process analysis and microbial ecology approach. PhD thesis. Department of Earth- and Life Sciences, Vrije Universiteit, Amsterdam. 140 pp.

Van Breukelen, B.M., Appelo, C.A.J., Olsthoorn, T.N., 1998. Hydrogeochemical transport modeling of 24 years of Rhine water infiltration in the dunes of the Amsterdam water supply. J. Hydrol. 209 (1–4), 281–296.

Van Breukelen, B.M., Röling, W.F.M., Groen, J., Griffioen, J., Van Verseveld, H.W., 2003. Biogeochemistry and isotope geochemistry of a landfill leachate plume. J. Contam. Hydrol. 65 (3–4), 245–268.

Van der Lee, J., de Windt, L., 2001. Present state and future directions of modeling of geochemistry in hydrogeological systems. J. Contam. Hydrol. 47 (2–4), 265–282.

Wajon, J.E., Ho, G.-E., Murphy, P.J., 1985. Rate of precipitation of ferrous iron and formation of mixed iron–calcium carbonates by naturally occurring carbonate materials. Water Res. 19 (7), 831–837.

Wiedemeier, T.H., Wilson, J.T., Kampbell, D.H., Miller, R.N., Hansen, J.E., 1995. Technical Protocol for Implementing Intrinsic Remediation with Long-term Monitoring for Natural Attenuation of Fuel Contamination Dissolved in Groundwater. U.S. Air Force Center for Environmental Excellence, Technology Transfer Division, Brooks Air Force Base, San Antonio, Texas. 643 pp.

Yager, R.M., Fountain, J.C., 2001. Effect of natural gas exsolution on specific storage in a confined aquifer undergoing water level decline. Ground Water 39 (4), 517–525.

Zhang, C.L., Horita, J., Cole, D.R., Zhou, J.Z., Lovley, D.R., Phelps, T.J., 2001. Temperature-dependent oxygen and carbon isotope fractionations of biogenic siderite. Geochim. Cosmochim. Acta 65 (14), 2257–2271.